BBA - Molecular Basis of Disease 1865 (2019) 165519

Contents lists available at ScienceDirect

BBA - Molecular Basis of Disease

journal homepage: www.elsevier.com/locate/bbadis

Low fluid shear stress conditions contribute to activation of cerebral cavernous malformation signalling pathways

Jia Li[a,d], Yang Zhao[a,d], Paul Coleman[a], Jinbiao Chen[b], Ka Ka Ting[a], Jaesung Peter Choi[c], Xiangjian Zheng[c], Mathew A. Vadas[a,d], Jennifer R. Gamble[a,d,*]

[a] Centre for the Endothelium, Vascular Biology Program, Australia
[b] Liver Injury and Cancer Program, Australia
[c] Laboratory of Cardiovascular Signalling, Vascular Biology Program, Centenary Institute, The University of Sydney, Camperdown 2007, NSW, Australia
[d] Sydney Medical School, The University of Sydney, Sydney, NSW, Australia

ARTICLE INFO

Keywords:
Cerebral cavernous malformations
Endothelial cells
Fluid hear stress
Inflammation
RNA sequencing

ABSTRACT

Cerebral cavernous malformations (CCMs) are vascular malformations that cause hemorrhagic stroke. CCMs can arise from loss-of-function mutations in any one of *CCM1* (*KRIT1*), *CCM2* or *CCM3* (*PDCD10*). Despite the mutation being in all endothelial cells the CCM lesions develop primarily in the regions with low fluid shear stress (FSS). Here we investigated the role of FSS in the signalling pathways associated with loss of function of CCM genes. We performed transcriptomic analysis on CCM1 or CCM2-silenced endothelial cells subjected to various FSS. The results showed 1382 genes were deregulated under low FSS, whereas only 29 genes were deregulated under high FSS. Key CCM downstream signalling pathways, including increased KLF2/4 expression, actin cytoskeleton reorganization, TGF-β and toll-like receptor signalling pathways and also oxidative stress pathways, were all highly upregulated but only under low FSS. We also show that the key known phenotypes of CCM lesions such as disrupted endothelial cell junction, increased inflammatory response/oxidative stress and elevated RhoA-ROCK activity, are only exhibited in monolayers of CCM-silenced endothelial cells subjected to low FSS. Our data establishes that shear stress acts as a previously unappreciated but important regulator for CCM gene function and may determine the site of CCM lesion development.

1. Introduction

Cerebral cavernous malformations (CCM) are vascular malformations that are prone to leakage, often leading to hemorrhagic stroke and seizures. Loss-of-function mutation in either one of 3 genes that form the CCM complex, *CCM1* (*KRIT1*), *CCM2*, and *CCM3* (*PDCD10*), results in the familial forms of the disease [1]. The CCM complex has been shown to be essential in control of vascular integrity [2–4], explaining the underlying vascular leak of the pathology [5,6].

One of the major unresolved questions in CCM pathology is the underlying mechanism for the selective locations of CCM lesions. In humans, although CCM genes are ubiquitously expressed, the development of CCM lesions is confined primarily to the CNS [5]. In animal models mimicking human CCM disease, despite pan-EC *Ccm* gene ablation, lesions form predominantly in the brain and retina [1] at a time when there is active angiogenesis [7]. These are regions with poor blood flow and low fluid shear stress (LSS) and indeed, in human and animal models, CCM lesions show sluggish blood flow [2–4].

Shear stress is caused by the drag force of blood flow, and plays an important role in the control of blood vessel growth and endothelial cell (ECs) functions [8]. Intriguingly, many of the CCM downstream pathways, including KLF2/4, RhoA-ROCK and TGF-β1, are activated by LSS [9–11]. Thus LSS may be an important secondary event in the induction of CCM lesions [12]. Although LSS has been speculated to play a role in the development of CCM [13], how FSS affects loss-of-CCM induced phenotypes and signalling pathways in EC has not been investigated systematically. In the present study, we explored whether shear stress impacts on the signalling pathways induced by loss of CCM1 or CCM2 in EC. Our results indicate that LSS is a prerequisite for loss-of-CCM induced key downstream signalling pathways.

2. Materials and methods

2.1. Mice

Cdh5^{Cre} *Ccm2*$^{fl/fl}$ animals have been previously described [14].

* Corresponding author at: Centre for the Endothelium, Vascular Biology Program, Centenary Institute, Locked Bag 6, Newtown, New South Wales 2042, Australia.
E-mail address: j.gamble@centenary.org.au (J.R. Gamble).

https://doi.org/10.1016/j.bbadis.2019.07.013
Received 14 December 2018; Received in revised form 18 June 2019; Accepted 27 July 2019
Available online 29 July 2019

Ccm2 EC specific knockout mice (*Ccm2*^{iECKO}) were obtained by crossing *Cdh5*^{Cre} and *Ccm2*$^{fl/fl}$ mice. To induce *ccm2* gene EC specific deletion in neonatal mice, 40 μg of 4-hydroxytamoxifen (4OHT, Sigma Aldrich) dissolved in corn oil was injected intragastrically to pups at P1. The Sydney Local Hospital District animal welfare committee approved all animal protocols.

2.2. Cell culture

HUVECs were isolated and cultured as previously described [15]. The umbilical cords were anonymous (donors non-identifiable) and informed consent was given for their use. The human cerebral microvascular endothelial cell line hCMEC/D3 were maintained in Endothelial Cell Basal Medium-2 (Lonza, Switzerland) supplemented by SingleQuots Kit (Lonza) [16]. Cells were cultured at 37 °C in a 5% CO2 humidified atmosphere.

2.3. Knockdown CCM1 and CCM2 in ECs by siRNAs

ECs were seeded at 2.0×10^5 cells in gelatin-coated 6-well plate wells or 4.0×10^4 cells in fibronectin-coated straight or Y-shape IBIDI Slide (IBIDI GmbH, Germany) overnight. Lipofectamine:siRNA (Thermo Fisher Scientific) complexes were formed by mixing 1.5 μL of Lipofectamine RNAiMax (Thermo Fisher Scientific), diluted in 150 μL OptiMEM (Thermo Fisher Scientific), and 1.5 μL of 10 μmol/L siRNA to control, CCM1 or CCM2, diluted in 150 μL OptiMEM, for 10 min. The complexes were added to 1.2 mL EBM-2 medium, and then added to cells on a plate or slide. Cells were incubated overnight, after which the medium was replaced with corresponding culture medium.

2.4. In vitro fluid shear stress

HUVEC grew to confluence on strait or Y-shape IBIDI slides 48 h after seeding. The ECs were then either kept under static or exposed to various shear stress conditions using IBIDI pump system (IBIDI GmbH). For RNA extraction, EC were harvested 2–24 h after various shear stress treatments.

2.5. Neutrophil adhesion assay

The live-cell microscopy flow model has been described [17,18]. Neutrophils were isolated as previously reported [19]. Confluent endothelial monolayers with or without CCM1 knockdown were stimulated with 5 ng/mL TNF-α (R&D system) for 2 h prior to shear stress treatment. Imaging was acquired using an inverted phase-contrast microscope (Nikon Eclipse TE2000), connected to a Nikon Digital Sight camera. Neutrophils (10^6 cells/mL in culture medium) were infused into the Y-shape IBIDI μ-Slide and allowed to settle for 10 min. Cells were imaged 10 min after introduction of 2 dyn/cm^2 constant shear stress. A gentle wash was given 20 min after application of shear stress. Images were then taken from different spots. Neutrophils per field were counted by Fiji ImageJ version 2.0.0-rc-34/1.50a.

2.6. Immunofluorescence and confocal microscopy

For immunofluorescence stain, cells were fixed for 15 min with 4% paraformaldehyde at room temperature or 50/50 (v/v) methanol/acetone at −20 °C, then permeabilised for 10 min with 0.1%Triton X-100 in Ca^{2+}/Mg^{2+} phosphate-buffered saline (PBS) followed by 2 h blocking with 2% bovine serum albumin (BSA) before probing with various antibodies. Primary antibodies used were: goat polyclonal anti-VE-cadherin (Santa Cruz Biotechnology), rhodamine phalloidin (Life Technologies), rabbit phospho-Myosin Light Chain 2 (Ser19) (Cell Signaling) and rabbit phospho-VEGFR2 Y1175 (Cell Signaling). Secondary antibodies included anti-rabbit Alexa Fluor 488, anti-goat Alexa Fluor 594 (Invitrogen). Cells were mounted with ProLong Gold Antifade Reagent (Invitrogen). Microscopy was performed with a Leica SP5 confocal microscopy (Leica Microsystems, Wetzlar, Germany). Images were analysed by using Fiji software. (Version: 2.2.2-rc-34/1.50a, NIH).

VE-cadherin staining was quantified as previously described with modification [20,21]. In brief, the total intensity of VE-cadherin was first measured by Image J [20]. The width of the junctions were determined by the line perpendicular to the widest gap per junction [21]. The intensity scores were then shown as intensity divided by width.

2.7. Measurement of superoxide formation

For ECs without FSS treatment, live HUVEC were incubated with the cell-permeant (0.1% triton X-100) and 3 μM dihydroethidium (DHE) (Thermo Fisher Scientific). Fluorescence microscopy was performed after a 30-min incubation. For ECs with FSS treatment, DHE was added to the medium 30 min prior to completion of a 4 h shear regimen [22,23]. Confocal microscopy was then performed as described beforehand.

2.8. RNA sequencing

Total RNA was extracted from ECs using RNeasy Plus Mini Kit (Qiagen). RNA-Seq libraries for mRNA profiling were prepared from 1.5 to 5 μg total RNA using the NEBNext® UltraTM RNA Library Prep Kit for Illumina® (NEB, USA) following manufacturer's recommendations. Library fragments were purified with AMPure XP system (Beckman Coulter, Beverly, USA). Library quality was assessed on the Agilent Bioanalyzer 2100 system. Library preparations were sequenced on an Illumina Hiseq4000 platform and 150 bp paired-end reads were generated. Reference genome and gene model annotation files were downloaded from genome website browser (NCBI/UCSC/Ensembl) directly. Indices of the reference genome were built using Bowtie (v2.2.3) and paired-end clean reads were aligned to the reference genome using TopHat (v2.0.12). We then used HTSeq (v0.6.1) to count the read numbers mapped of each gene, followed by calculation of RPKM (Reads Per Kilobase of exon model per Million mapped reads) of each gene based on the length of the gene and reads count mapped to that gene. Differentially expressed genes were then determined using DESeq R package (v1.12.0). The resulting P-values were adjusted using the Benjamini and Hochberg's approach for controlling the False Discovery Rate (FDR). Genes with an adjusted P-value < 0.05 and FDR < 0.005 were assigned as differentially expressed.

2.9. Gene set enrichment and protein-protein interaction analysis

Modified gene set enrichment analysis (GSEA) was used to assess functional significance at the level of sets of genes as previous described [24]. All of these potential targets were compared with the "c2_all" collection of curated gene sets from the Molecular Signatures Database (v6.1), consisting of 1077 gene sets corresponding to BIOCARTA (217), KEGG (186) and REACTOME (674) biological pathways. Heat maps were generated using the Multiple Array Viewer MeV_4_8 (version 10.2).

Protein-protein interaction analysis of differentially expressed genes was processed by the web-based STRING analysis (v10.5), which contained known and predicted Protein-Protein Interactions. We constructed the networks by extracting the target gene lists from the database.

2.10. RNA isolation and quantification of gene expression using quantitative reverse transcription PCR

Total RNA, including small RNA fraction was extracted from ECs using miRvana RNA isolation kit or Trizol (Thermo Fisher Scientific) [15]. RNA was isolated for each condition and two steps real-time RCR was used to measure miRNAs. First, 1 μg of RNA was reverse

transcribed to cDNA by using reverse transcription kit, followed by TaqMan probe based real time PCR (Life technologies). The relative RNA amount was calculated with the $2^{-\Delta\Delta CT}$ method [24]. All reactions were performed in quadruplicates and repeated in three biological replicates using Biorad real-time PCR machine (Biorad).

2.11. Preparation of cell extracts and Western blotting

Western blot analysis was performed as previously described [15] Whole-cell lysates were prepared using lysis buffer 1 mol/L Tris HCl, pH 7.5, with 1% NP-40, 5 mol/L NaCl, 200 mmol/L EGTA, 500 mmol/L NaF,100 mM $Na_4P_2O_7$ containing 1× protease inhibitor cocktail (Sigma Aldrich). Equal amounts of protein were loaded onto a 4–15% precast polyacrylamide gel (BioRad) and separated by electrophoresis in a running buffer, and then transferred to PVDF (polyvinyl difluoride) membranes in transferring buffer, blocked with 5% skim milk powder in PBS-Tween 20 (0.05%). The membranes were probed with ICAM-1 rabbit (1:1000, 4915, Cell Signalling) and α-tubulin (Santa Cruz) overnight at 4 °C or for 1 h at room temperature, followed by corresponding HRP-conjugated antibody (1:5000; Amersham, UK) for 1 h at room temperature. Proteins were visualized using ECL Western blotting Detection Reagents (GE Healthcare, Little Chalfont, UK) on ChemiDoc MP system (Bio-rad). Densitometric analysis was performed using ImageJ (Version 1.48, NIH, USA) software.

2.12. Statistics

All experiments were not assessed blindly. Sample size determination was based on previous experience with similar studies. The researchers were not blinded to the treatment groups when performing experiments and data assessment. Data are expressed as mean ± standard deviation (SD) for the indicated number of observations. P values were calculated as indicated in figure legends using an unpaired, two-tailed Student's *t*-test or one-way ANOVA with Tukey correction for multiple comparisons. A P value of < 0.05 was considered significant.

2.13. Study approval

Human umbilical cords were collected under approval from the New South Wales Local Sydney Health District Ethics Committees. This study was conducted in accordance with the Declaration of Helsinki.

2.14. Key resources table

Resource	Source	Identifier
Antibodies		
anti-goat Alexa Fluor 594	Thermo Fisher Scientific	N/A
anti-rabbit Alexa Fluor 488	Thermo Fisher Scientific	N/A
a-tubulin	Cell Signaling Technology	N/A
goat polyclonal anti-VE-cadherin	Santa Cruze Biotechnology	N/A
Cell Line		
hCMEC/D3	N/A	N/A
HUVEC	N/A	N/A
Chemical		
4-hydroxytamoxifen		Sigma Aldrich
acetone	Sigma Aldrich	N/A
DHE	Thermo Fisher Scientific	N/A
dihydroethidium	Thermo Fisher Scientifc	N/A
EGTA	Thermo Fisher Scientifc	N/A
methanol	Sigma Aldrich	N/A
phalloidin	Thermo Fisher Scientific	N/A
phosphate-buffered saline	Sigma Aldrich	N/A
Tris	Fluka	N/A
Triton X-100	Fluka	N/A
Protein Peptide		
protease inhibitor	Sigma Aldrich	
TNF-a	R&D System	

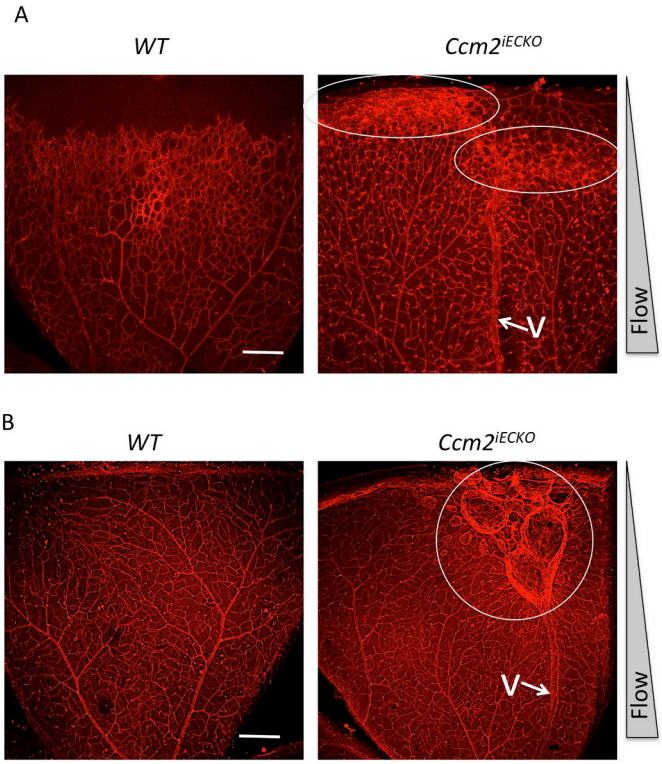

Fig. 1. Effects of blood flow on the development of retinal CCMs under impaired CCM2 signalling.
Representative images of P7 (A) and P31 (B) retinas stained with isolectin B4 to identify blood vessels in control (WT) and *Ccm2*^{iECKO} mice after tamoxifen treatment at P1. V: vein. CCM lesions are the areas marked by circles. Shear stress is higher in the area close to the optic nerve and decreases towards the periphery of the vascular plexus. Scale bars, 200 μm.

3. Results

3.1. CCM lesions in retina occur in regions of low blood flow

In line with previous report, in the retina of 7-day-old (P7) (Fig. 1A) and 31-day-old (P31) (Fig. 1B) *Ccm2* endothelial specific knockout mice, CCM lesions present at the vein and periphery of venous plexus in retinas [1,25] (Fig. 1). These are regions in the retina vasculature where blood flow and FSS is the low [25–27]. The arteries, where blood flow is higher, were thin and normal (Fig. 1) [28]. Thus, loss of *Ccm2* results in the abnormal vascular remodelling specifically in regions of low blood flow. These results suggested that blood flow induced shear stress may contribute to loss-of-CCM induced downstream signalling.

3.2. Silence of CCM2 induced KLF2/4 upregulation is dependent of shear stress magnitude

KLF2/4 act downstream in the CCM pathway and are essential in the development of CCM lesions [14,29]. KLF2/4 are also widely reported as FSS induced genes [10,11].To investigate how FSS affects loss-of-CCM gene induced signalling pathways, we first examined KLF2/4 expression in CCM2-silenced EC subjected to various FSS from 0 to 15 dyn/cm^2. HUVECs were used in most of the experiments, as a model system as they have been widely used to explore the effect of FSS on ECs and loss-of-CCM induced signalling pathways [10,29–33]. They can be obtained in sufficient quantities to negate the need for extended passage in culture or viral transformation, both of which result in substantial changes in cell-cell junctions and other endothelial cell characteristics. siRNA to CCM1 and CCM2 resulted in > 90% depletion

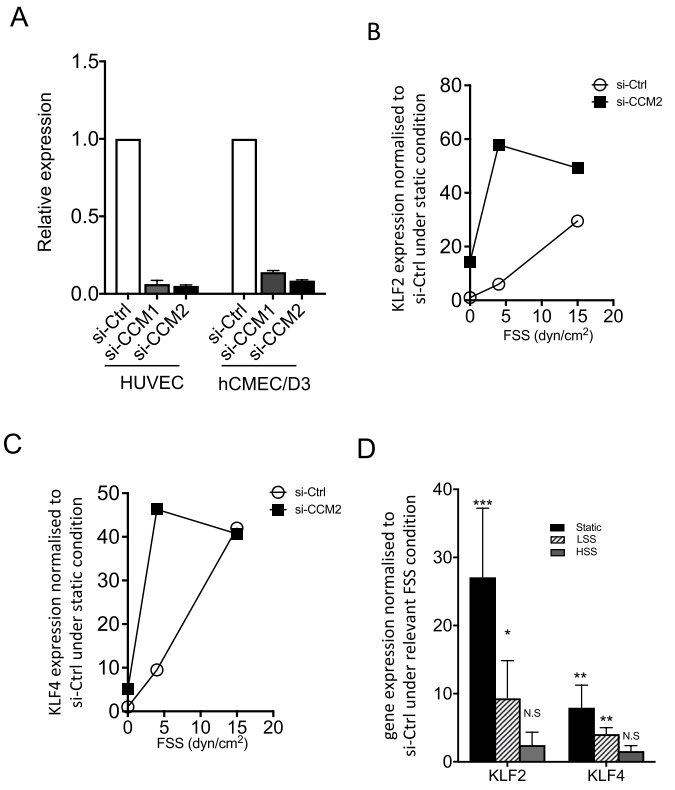

Fig. 2. Upregulation of KLF2/4 is dependent on the magnitude of the shear stress. (A) siRNA to CCM1 or CCM2 markedly reduces CCM1 or CCM2 expression in two types of ECs, HUVEC or brain microvessel ECs (hCMEC/D3). (B) KLF2 and (C) KLF4 expression in control (si-Ctrl) and CCM2-silenced EC (si-CCM2) at each of the FSS conditions. Expression is relative to the level in control EC under static condition. Results are a single experiment representative of n = 4–5 independent experiments. (D) Pooled data of n = 4–5 independent experiments, of KLF2 and KLF4 expression levels normalized to si-Ctrl treated EC under the relevant static, LSS or HSS conditions. Data represents mean ± SD *P < 0.05, **P < 0.01, ***P < 0.001, N·S: not significant, determined by one-way ANOVA with Tukey correction.

of the mRNA in both HUVEC or hCMECs (Fig. 2A).

Under static conditions (FSS = 0), and consistent with previous reports [29,34], KLF2/4 were lowly expressed in control cells but massively increased with silencing of CCM2 (a representative HUVEC line, Fig. 2B,C), giving a roughly 25 fold ratio (KLF2) and 8 fold ratio (KLF4) between these two conditions (pool of 4–5 HUVEC lines, Fig. 2D). Under high FSS (HSS 15 dyn/cm^2), although KLF2/4 expression was increased in both CCM2 depleted and control cells, the difference between these two groups was diminished (Fig. 2B,C) to a ratio without statistical significance (Fig. 2D). In the intermediate LSS conditions (3.5 dyn/cm^2), KLF2/4 expression in CCM2 depleted cells was still much higher than that of control cells (Fig. 2B,C), with a ratio of roughly 9 for KLF2 and 5 for KLF4 (Fig. 2D). It is also noteworthy that in CCM2-silenced cells, maximum levels of KLF2/4 were induced under LSS, and the levels were not changed with a further increase in FSS (Fig. 2B,C). This is different to the case in the high flow vascular malformation disease: hereditary hemorrhagic telangiectasia, where KLF2/4 are significantly higher under both static and HSS [27]. These results suggest a hyper-responsiveness of KLF2/4 expression to flow in the absence of CCM2.

3.3. Silencing of CCM2 in the context of different FSS results in distinct transcriptomic profiling

The above results suggested that CCM gene loss may allow an inappropriate expression of genes under LSS. To test this hypothesis, we applied RNA-seq based transcriptomic analysis to control or CCM2-silenced EC, subjected to either LSS or HSS.

As anticipated there was a marked difference in the gene expression pattern of control ECs between LSS and HSS conditions (comparison 1) (Fig. 3A), with 1189 genes increased and 32 genes decreased. The regulated genes included those previously reported as increased in ECs by HSS such as *SIRT1* [35], *ITGB1* [36] and *HMGB1* [37], and decreased in ECs subjected to HSS such as *IGFBP7* [38]. These genes are important for proper vascular functions [35–38]. Thus, our model was detecting flow and the cells were responding in the anticipated manner.

The pattern was also strikingly different between control and CCM2-silenced cells under LSS (LSS-CCM) (Comparison 2 Fig. 3A) with 1382 genes (≥2-fold change) differentially expressed (Fig. 3B). In sharp contrast, in CCM2-silenced cells under HSS (HSS-CCM), only 29 were differentially expressed (Comparison 3, Fig. 3A and C). Since KLF2 is higher in LSS-CCM but not HSS-CCM (Fig. 2), the possibility existed that the deregulated genes under LSS-CCM maybe KLF2-regulated genes. To exclude this possibility, we performed a cross-validation with 373 deregulated genes induced by KLF2 overexpression in EC as previously reported [10]. Of these 373 genes, only 16 of these were also induced under LSS-CCM (Fig. 3D). This would suggest that KLF2 is not a major regulator of the differentially expressed genes under LSS-CCM. Overall, this data suggests that shear stress may play a critical role in the gene profiles conferred by loss-of-CCM2.

3.4. Effects of FSS on key loss-of-CCM2 induced pathways

We then investigated signalling pathways for the dysregulated genes under LSS-CCM. Of the 1382 genes that were differentially expressed under LSS-CCM (Comparison 2), 1281 genes were upregulated, whereas only 9 genes were upregulated under HSS-CCM (Comparison 3) (Fig. 4Ai). Those upregulated genes in the LSS conditions, included *ROCK1/2*, *TGFB2*, *TGFBR1*, *MYCBP*, *ITGB1* and *AKT3*, all involved in CCM-related pathways, such as the actin cytoskeleton, WNT, TGFβ and VEGF signalling pathways (based on KEGG, Kyoto Encyclopedia of Genes and Genomes analysis) (Fig. 4Ai, ii, Supplemental Tables 1, 2 and Supplemental Fig. 1A–C) [2,3,5,29,39,40].

Our approach also allowed us to discover potential new pathways associated with CCM development. A notable result was that a large number of genes were enriched in gene sets involved in host-defence and inflammatory responses (Fig. 4Aiii). Among these gene sets are Toll-like receptors, NOD-like receptors and RIG-I-like receptors signalling pathways, which are crucial for sensing microbiota-derived pathogens peptidoglycan (PGN) fragments and endogenous danger-associated molecules in the bloodstream [41,42]; Endocytosis signalling pathway facilitating PGN across endothelial host barriers [42]; Nuclear factor κB (NF-κB) and MAPK signalling pathways involved in the transcriptional upregulation of pro-inflammatory and host-defence genes. These results are in line with a recent report showing gut microbiome contributes to CCM pathology where TLR4 was involved [39] (Supplemental Fig. 1D). Other gene pathways not previously implicated in CCM pathology but regulated in our data set, include the NF-κB activators *TBK1* and *TANK* [43]; *XIAP*, *BIRC2* and *TAB2* involved in NOD like receptor signalling pathway for gene activation [42] (Fig. 4Aiii). We have validated some of the genes identified in our screen and known to be involved in CCM development, including *RhoA*, *HIF1α*, *TLR4* and *TGFβ1* (Fig. 4B), thus confirming the validity of our screen.

Whilst the downregulated gene numbers were less impressive there were some interesting changes. 101 of 1382 altered genes were downregulated under LSS-CCM (Fig. 3, Comparison 2) whereas under HSS-CCM only 20 genes were regulated (Fig. 3, Comparison 3), with 13 genes in common between these two data sets (Fig. 4Ci). Gene set analysis of the 101 downregulated genes showed an enrichment in genes involved in vascular development and angiogenesis under both LSS-CCM and HSS-CCM (Fig. 4Cii) suggesting CCM2 is required for

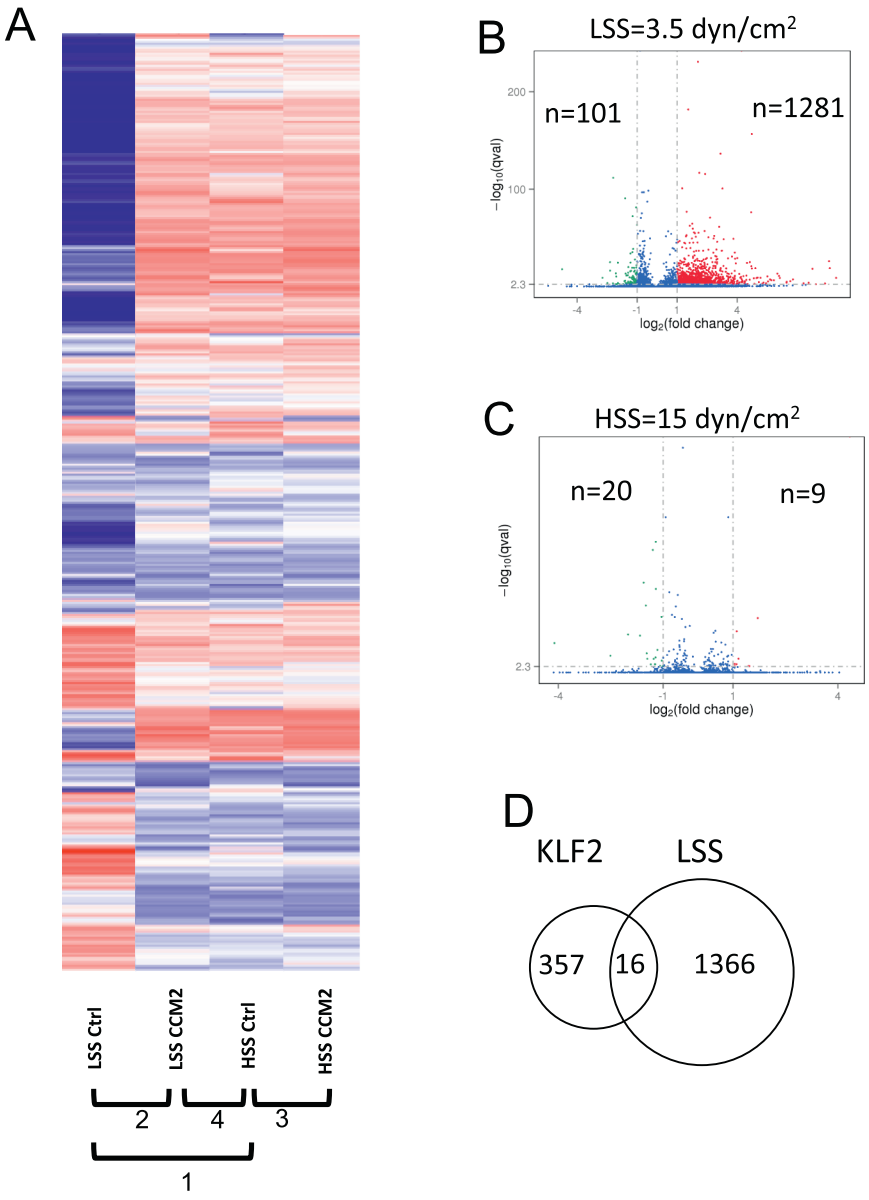

Fig. 3. Silencing of CCM2 under different FSS results in distinct transcriptomic profiling. (A) Heatmap representing gene expression level. Red denotes genes with high expression levels, and blue denotes genes with low expression levels. (B and C) Cuffdiff analysis showing the differentially expressed genes between control and CCM2-silenced EC under LSS (B) and HSS (C). The x-axis shows the fold change in gene expression between different samples, and the y-axis shows the statistical significance of the differences. Significantly up and down (> 2-fold change) regulated genes are highlighted in red and green, respectively. Genes that were similar in expression (< 2-fold change) between treatment group and control group are in blue. (D) Venn diagram of differentially expressed genes in common between genes induced by KLF2 overexpression and by silence of CCM2 under LSS. The numbers in each circle is the total number of genes expressed within a group, and the overlap represents the genes expressed in common between groups. (For interpretation of the references to color in this figure legend, the reader is referred to the web version of this article.)

vascular development regardless of the FSS magnitude. This is consistent with reports that CCM2 is required for proper assembly of head, heart and intersomitic vasculature [34]. Further, of the 101 genes downregulated under LSS-CCM, some are involved in the pathways that contribute to CCM pathology, such as *NOTCH1* [25] and its downstream target, *HES4* [44] and also a decrease in the anti-oxidant gene, GPX1 [45–47]. In line with the loss of claudin-5 and decreased pericyte coverage in the EC lining CCM lesion, *SOX18*, a transcription factor regulating Claudin-5 expression [48], and *PDGFB*, a key molecule involved in pericyte-endothelial interaction [49] are both down-regulated (Fig. 4Ciii, D).

3.5. Loss-of-CCM2 induced RhoA-ROCK activity and actin reorganization is dependent on shear stress magnitude

To further confirm FSS as an important component of loss-of-CCM induced phenotypes, we investigated, under different FSS, the regulation of the hallmark of CCM development, the increase in RhoA/ROCK activity [2,14]. The RhoA-ROCK pathway was evaluated by staining for pMLC and evaluating stress fibre content. In line with previous reports [2,14], silencing CCM2 resulted in higher levels of pMLC under static condition (Fig. 5Aiv vs. i, and 5C). Under LSS conditions (3.5 dyn/cm^2), there was the anticipated increase in pMLC (Fig. 5Aii vs. i, 5C) in control cells. LSS-CCM cells showed similar elevated levels of pMLC when the cells were under LSS for either 1.5 or 24 h (Fig. 5Av vs. ii, vi vs. iii, 5C). However, this difference disappears when cells were subjected to HSS for either 1.5 or 24 h (Fig. 5B), with the level of pMLC staining in CCM2-silenced EC reducing to a level similar to control EC (Fig. 5Bv, vi, 5C). Thus the changes, due to CCM2 silencing are only observable under LSS. Similar effects were seen for F-actin stress fibres (Fig. 5D). Under static conditions, silencing of CCM2 increased the formation of F-actin stress fibres (Fig. 5Div vs. i) [2] with the differences disappearing under HSS (Fig. 5Dv vs. ii, vi vs. iii, 5C). Thus, HSS rescues the effects on F-actin stress fibres caused by silencing of CCM2 (Fig. 5Dvii), confirming the vascular protective effects of HSS [50].

3.6. CCM2-silencing induced ECs junction disruption and inflammatory reaction is dependent of shear stress magnitude

We then investigated the effect of FSS on two other hallmarks of CCM including ECs junctional reorganization [5,25], and inflammation [5]. On the Y shape slide, FSS varies with position, with LSS seen in

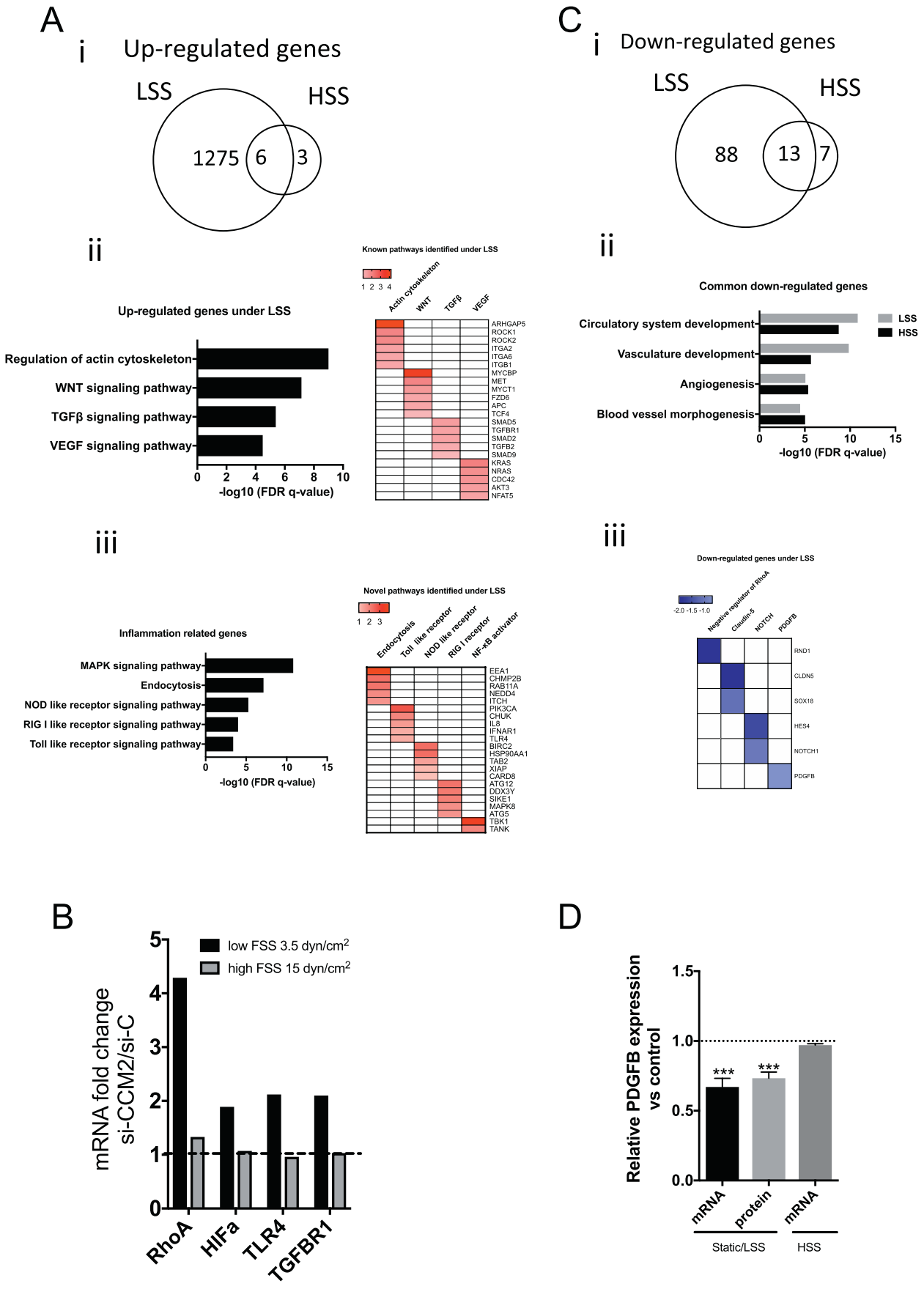

Fig. 4. Pathways and genes deregulated in CCM2-silenced EC. (A) Venn diagrams showing the number of genes upregulated under LSS and HSS (i). Hallmark gene sets/pathways enriched for upregulated mRNAs in CCM2-silenced EC under LSS(ii, iii). (B) The mRNA expression of *RhoA*, *HIFa*, *TLR4* and *TGFBR1* was quantified by real-time PCR. (C) Venn diagrams showing the number of genes downregulated under LSS and HSS(i). Common hall-mark gene sets enriched in CCM2-silenced EC under both LSS and HSS (ii). Key downregulated genes under LSS (iii). (D) *PDGFB* mRNA and protein expression in CCM2-silenced EC under static/LSS and HSS condition.

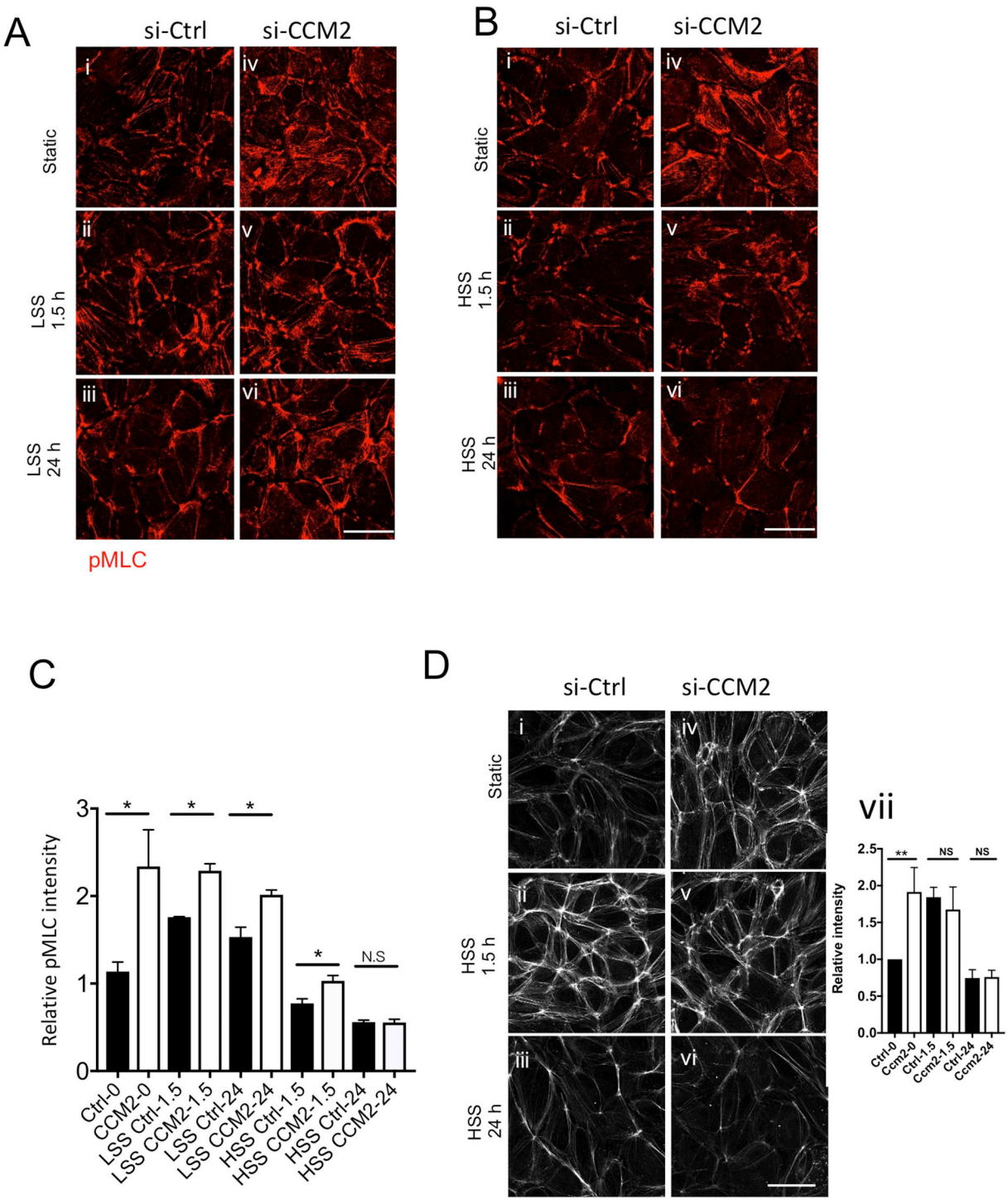

Fig. 5. CCM2 depletion induces RhoA activity that is dependent on the magnitude of the shear stress. RhoA activity as shown by staining of pMLC under LSS (A) or HSS (B). (C) Quantification of phospho-MLC intensity in (A) and (B). (D) Phalloidin staining for cellular actin fibres after static or HSS treatment. Results are representative of three independent experiments. Scale bars, 60 μm. Data represents mean ± SD *P < 0.05, **P < 0.01, N·S: not significant, determined by Student's *t*-test.

area1 and HSS in area 2 on the same slide [51] (Fig. 6A). In CCM2-silenced cells under static conditions the junctions were weaker and disorganized as shown by VE-cadherin staining (Fig. 6A iv vs. i). In the LSS region (Area 1, predicted FSS is 0–5 dyn/cm^2), the CCM2-silenced cells show wide, discontinuous and diffuse staining for VE-cadherin (Fig. 6Av), whereas control cells show a continuous VE-cadherin staining with a closed zipper-like appearance, indicative of tightly apposed junctions (Fig. 6Aii). In contrast, in the HSS (Area 2, 15 dyn/cm^2) region, both control and CCM2-silenced ECs showed less disruption in VE-cadherin junctional staining and fewer gaps (Fig. 6Aiii and vi), consistent with the known effect of HSS [50]. Indeed, the abundance of VE-cadherin was similar between CCM2-silenced ECs and control (Fig. 6Avii). Taken together, the results show that CCM2 is required for ECs to form tight junctions under LSS.

Silencing of CCM1 or CCM2 in ECs resulted in a significant upregulation of ICAM-1 (Fig. 6B), an inflammation marker known to

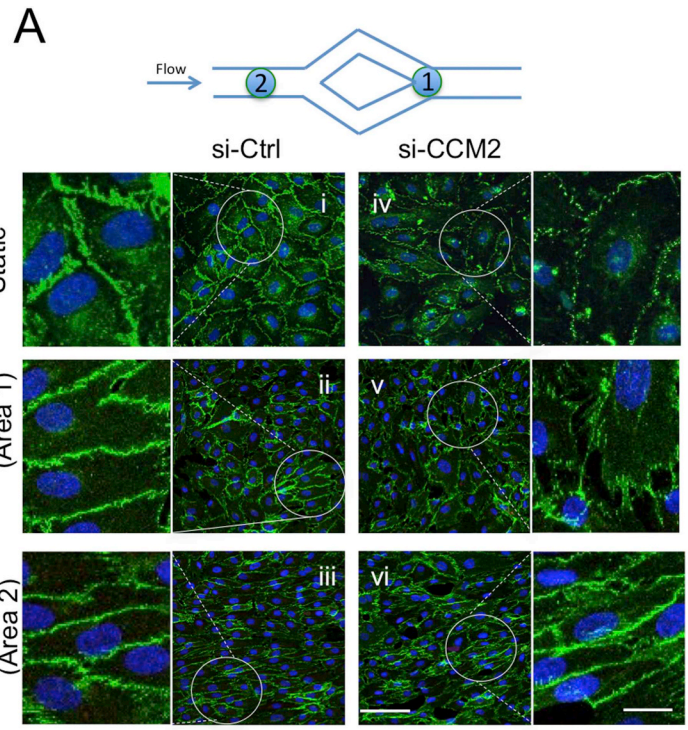

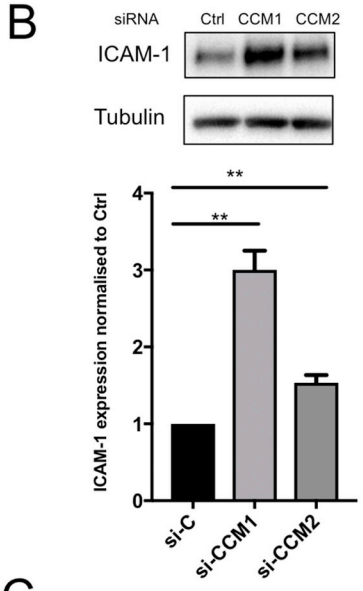

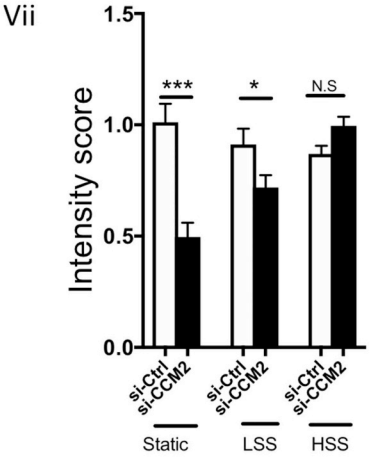

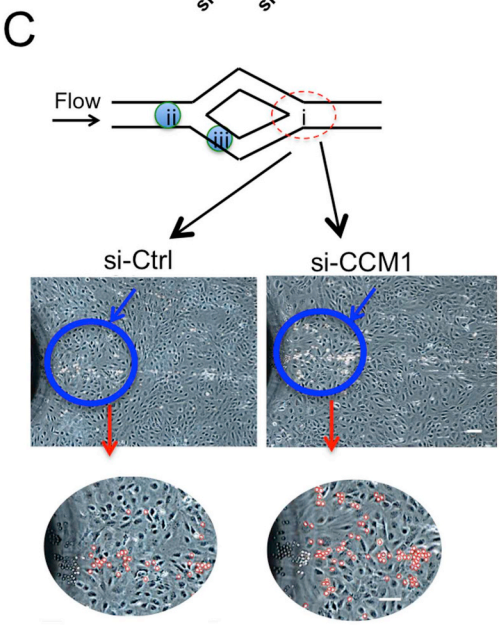

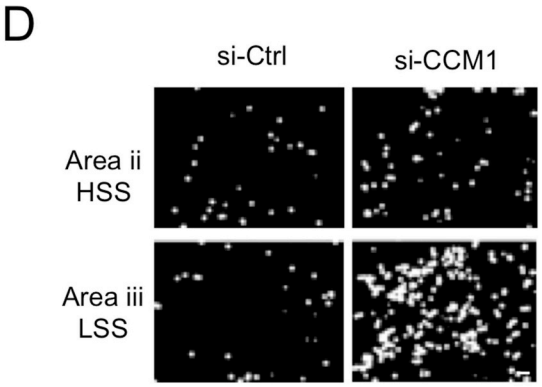

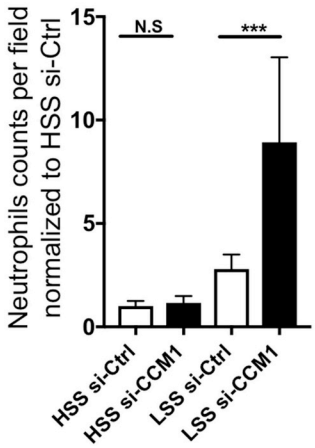

(caption on next page)

Fig. 6. CCM2 depletion induces disruptive EC junctions and enhanced inflammation that is dependent on the magnitude of the shear stress.
(A) ECs with or without siRNA-CCM2 treatment were plated on a Y-shape slide and stained for VE-cadherin, as an indicator of EC junctional integrity. Area 1 and 2 are subjected to LSS and HSS, respectively. Results are representative of 3 independent experiments. Scale bars, 60 μm and 250 μm(i–vi). VE-cadherin fluorescence intensity was divided by width to get intensity score (vii). (B) Western blot analysis of ICAM-1 expression with quantification of n = 4 independent experiments. (C) Microscopic images at the 45 degree branching area (area i) showing neutrophils adhering to hCMEC/D3 as assessed by *in vitro* adhesion assay. Red circle indicates neutrophils. (D) Neutrophil adhesion was quantified as the number of adherent neutrophils per field of view at uniform laminar but at 100% (area ii) and 50% (area iii) flow velocity regions in ibidi flow chambers. Scale bars, 60 μm. Means ± SD of 3 experiments reflect neutrophil counts from 5 fields per well. **P < 0.01, ***P < 0.001, N·S: not significant, determined by Student's *t*-test.

facilitate neutrophil adhesion and also regulated by FSS [18]. We investigated neutrophil adhesion in CCM1-silenced cells as knockdown of CCM1 resulted in more upregulation than CCM2 (Fig. 6B), In area i FSS continuously increased from left to right [51], and neutrophils preferentially attached to the lower FSS region (blue circle) in CCM1-silenced ECs (Fig. 6C). In Areas ii and iii uniform laminar flow is seen in both areas but FSS in area ii is twice the FSS in area iii [51]. ECs in HSS regions (area ii) captured similar numbers of neutrophils between control and CCM1-silenced ECs (Fig. 6D). However, in LSS region (area iii), there was a significant increase in the number of neutrophils adherent to CCM1-silenced ECs (Fig. 6D). Thus, LSS predisposes CCM-silenced ECs to increased adhesion of neutrophils following stimulation with the inflammatory cytokine, TNF.

3.7. CCM2 silencing induces oxidative stress under LSS

A further hallmark of CCM is increased oxidative stress in EC [13,52,53]. FSS has also been shown to regulate oxidative stress in EC [54,55]. Therefore, we investigated whether oxidative stress upon CCM-depletion is flow responsive.

The RNA-seq data showed that some oxidative stress and redox-sensitive pathways were up-regulated under LSS but not HSS. These included NF-κB and KLF2/4. In addition, the PI3K-Akt pathway (Supplemental Table 1), which lies upstream of NADPH oxidase 2 and reactive oxygen species (ROS) [28] was also upregulated by loss-of-CCM only under LSS. Further, HIF1a (Fig. 1B) and NF-kB related genes which lie downstream of NAPDH/ROS (Fig. 4Aiii) were also upregulated. These results imply that the oxidative stress pathway is highly upregulated by loss-of-CCM under LSS but not HSS.

To further the link between oxidative stress induction and LSS, we directly measured intracellular $O2^{-\cdot}$ production in CCM depleted EC under various FSS conditions. In line with previous reports [52,53], knockdown of CCM1 or CCM2 in HUVEC under static conditions increased intracellular $O2^{-\cdot}$ production, shown by DHE staining [52,53] (Fig. 7Ai, upper panel). Although LSS showed little change in the DHE level under static conditions (Fig. 7Ai, middle panel), HSS markedly inhibited the DHE level (Fig. 7Ai lower panel, Fig. 7Aii).

Our RNA-seq data also showed regulation of GPX1 [45,46], a crucial antioxidant gene. *GPX1* was decreased under LSS but not HSS in CCM2 depleted EC (Fig. 7Bi). This result was confirmed by real-time qPCR in CCM1 or CCM2 silenced EC under varying FSS condition. (Fig. 7Bii). Collectively, these results suggest HSS but not LSS rescues the effects on oxidative stress caused by silencing of CCM2.

3.8. Loss of CCM2 enhances mechanotransduction sensitivity under LSS

FSS selectively upregulates ICAM-1 and downregulates VCAM-1 [56,57]. Silencing CCM2 also regulates ICAM-1 and VCAM-1 with the same trend, together with KLF2/4 (Fig. 8A). Thus, there is a similarity of response in ECs to FSS and to CCM2 depletion. Indeed, LSS-CCM2 ECs have highly comparable transcriptomic profiling with only 1 gene significantly differently expressed (P-value < 0.05; FDR < 0.005; ≥2-fold change) to the control ECs under HSS (Fig. 3A, Comparison 4). Thus, in the absence of CCM2, the response to LSS by the ECs is similar to those under HSS, which will be inappropriate. Since ECs sense FSS via a range of molecular mechanosensors, these results indicate that loss-of-CCM may cause an alteration in the mechanosensing apparatus.

FSS sensors in ECs include integrins [8], PECAM1 and VEGFR2 [58,59], and Tie-2 [60]. Loss of CCM2 is known to activate integrin β1 [29,61]. We measured VEGFR2 and Tie-2, after CCM2 deletion. Under static and LSS conditions, silencing of CCM2 resulted in a significantly increased expression of VEGFR2 and Tie-2 (Fig. 8B). Although HSS increases gene expression in control ECs, there was significantly less change in CCM2-silenced ECs. These results indicate that loss of CCM genes may increase ECs sensitivity to LSS via altering mechanosensor gene expression. Acute flow treatment also triggers fast activation and nuclear translocation of the VEGFR2 tyrosine kinase as a response of ECs [62]. This reaction is critical to mediate the transduction of shear-stress signals into ECs [62]. In line with increased expression of VEGFR2 (Fig. 8B), loss of CCM2 also translocated Tyr1175 VEGFR2 to the nucleus (Fig. 8C), suggesting loss of CCM2 in ECs may sensitize the endothelium to FSS through increasing the levels and activity of mechanosenory complex genes.

4. Discussion

CCM lesions occur in the brain and retina, regions of low blood flow [12]. Despite recent progress in our understanding of CCM, only a limited number of pathways have been identified which are involved in the development of CCM lesions [2,5,14,29,33,39,63,64]. Further, the understanding of the site-restricted development of the CCM lesions has not been explained. We propose that shear stress contributes to the site restricted development of lesions in conditions of CCM loss-of-function. In support of this, we demonstrate, by RNA-sequence transcriptomic analysis, that CCM-silencing under LSS but not under HSS induces genotypic changes consistent with CCM lesion development. We further show that the disrupted junctions, enhanced neutrophil adhesion and induction of oxidative stress following CCM silencing occurred only under LSS but not under HSS. Finally, we show that LSS, facilitated changes in the expression of key molecules previously described in the response to flow in EC where CCM1 or CCM2 were silenced. Mechanistically, loss of CCM alters the expression of genes known to be mechanosensors, thus suggesting that the endothelium inappropriately responds to the FSS in the vessels within the regions of low blood flow. Our data demonstrates a new model, that loss of CCM sensitizes EC response to LSS in the capillary-venous vessels in retina and brain [65,66]. In accordance with our findings, CCM1 has been shown to control the sensitivity of ECs to hemodynamic forces during cardiovascular development [67]. We further suggest that LSS is a major determinant of the development of the CCM lesions in the CNS.

Silencing of CCM2 in EC placed under HSS did not lead to a significant change in gene expression compared to control cells. This was demonstrated, under HSS, by lack of morphological changes in the state of the junctions and by there being only 29 genes differently expressed between control and CCM2-silenced ECs (> 2.0 fold change). Even when we used ≥1.5-fold change as a cut-off, there were still only 92 genes changed under HSS. In contrast silencing of CCM2 under LSS resulted in loss of junctional integrity and 2034 genes were differentially regulated (> 1.5 fold). Thus, in the loss-of-function of CCM the effect on the endothelium will be site specific, at least partially governed by the FSS. In arteries, where FSS is high, we predict that loss of CCM will not cause major phenotypic changes. In contrast, EC in brain

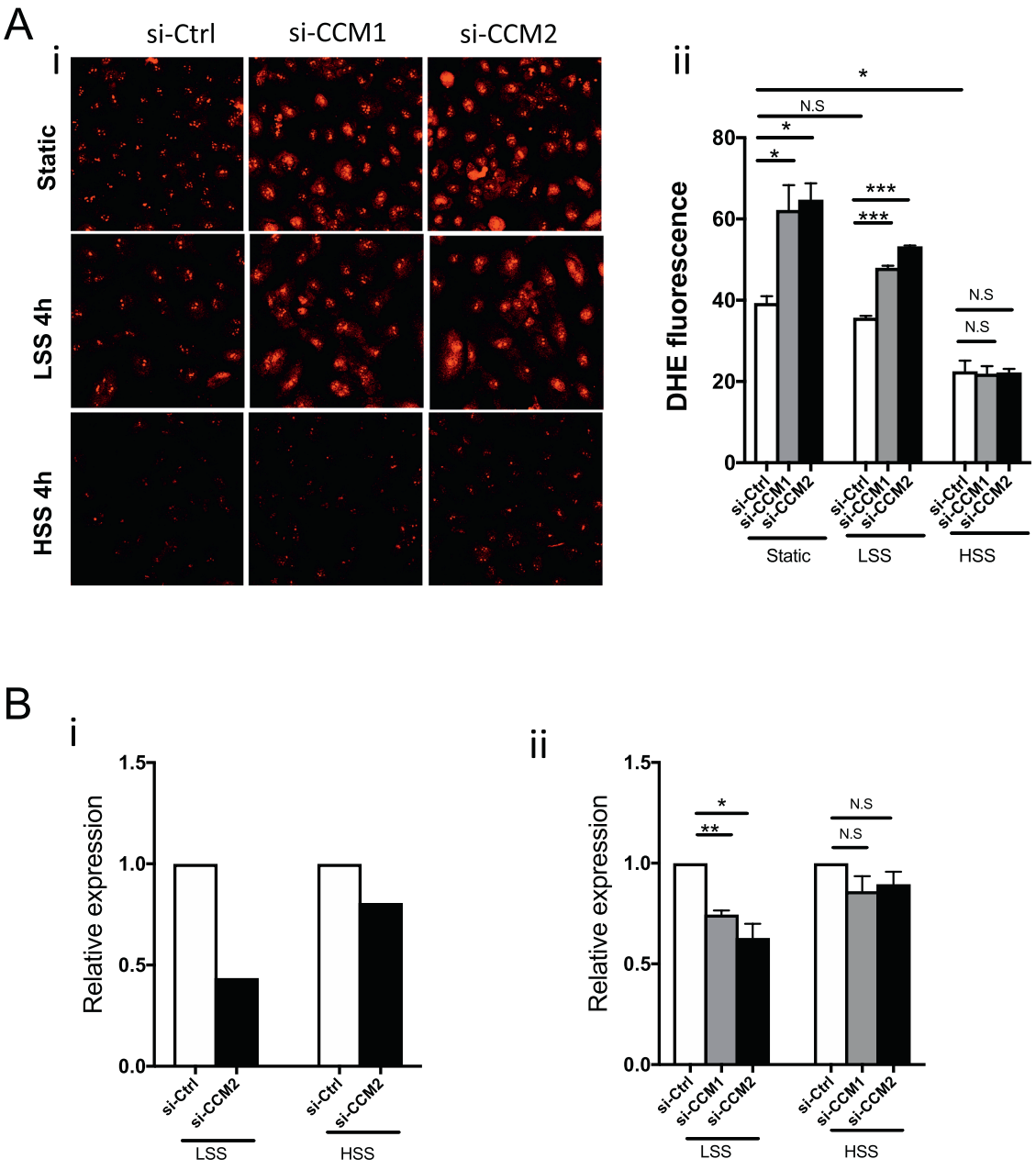

Fig. 7. Oxidative stress induced by depletion of CCM2 is rescued by high shear stress.
(A) (i) DHE fluorescence in negative control (si-ctrl), CCM1 or CCM2 depleted EC under static, LSS or HSS for 4 h. Images are representative of 4 independent experiments. (ii) Average DHE intensity per field of view given as mean ± SD of 5 experiments. (B) (i) *GPX1* levels in CCM2-depleted ECs under LSS from the RNA-seq analysis, and (ii) confirmed by real-time qPCR in CCM1 or CCM2 depleted EC under various conditions. Data is shown as mean ± SD of 5 experiments. *P < 0.05, ***P < 0.001, N·S: not significant determined by one-way ANOVA with Tukey correction.

capillaries, being subjected to LSS, CCM2 is essential to exert its protective effect.

Our in vitro flow model also offers a unique tool to identify new pathways contributing to CCM development. Firstly, GSEA analysis (Supplementary Table 1) revealed 116 of 1281 upregulated genes are involved in immune system gene set, suggesting a broader involvement of the immune response than previously considered [68]. Indeed, pathogen-infection and inflammation related signalling pathways are highly enriched in CCM2-silenced EC under LSS but not under HSS. Recently, the gut-bacterial triggered signalling, including but not limited to LPS-TLR4 signalling pathways, was shown to be a critical driver of CCM formation [39]. Our results suggest that under LSS, silence of CCM2 itself can trigger a pathogen-infection-like response in EC, or at least prime the endothelium towards such a response. Signals from the gut microbiome may then act as a second hit to strengthen the pathogen-infection like response in LSS areas, such as the CNS, to trigger or accelerate CCM development.

Secondly, CCM lesions are characterised by dilated capillaries [14]. The RNA-seq data showed upregulation in the CCM2-silenced cells under LSS of many genes associated with outward remodelling or negative regulation of vasoconstriction, namely *NOS3*, *MMP9*, *TWF1*, *HIF1A*, and *LEPR* [69–71]. In contrast, *PDGFB*, shown to induce inward remodelling [72], was significantly downregulated. This could also explain the loss of pericyte coverage in CCM lesions since PDGFB expression contributes to the recruitment of pericytes to vessels [49,73–75].

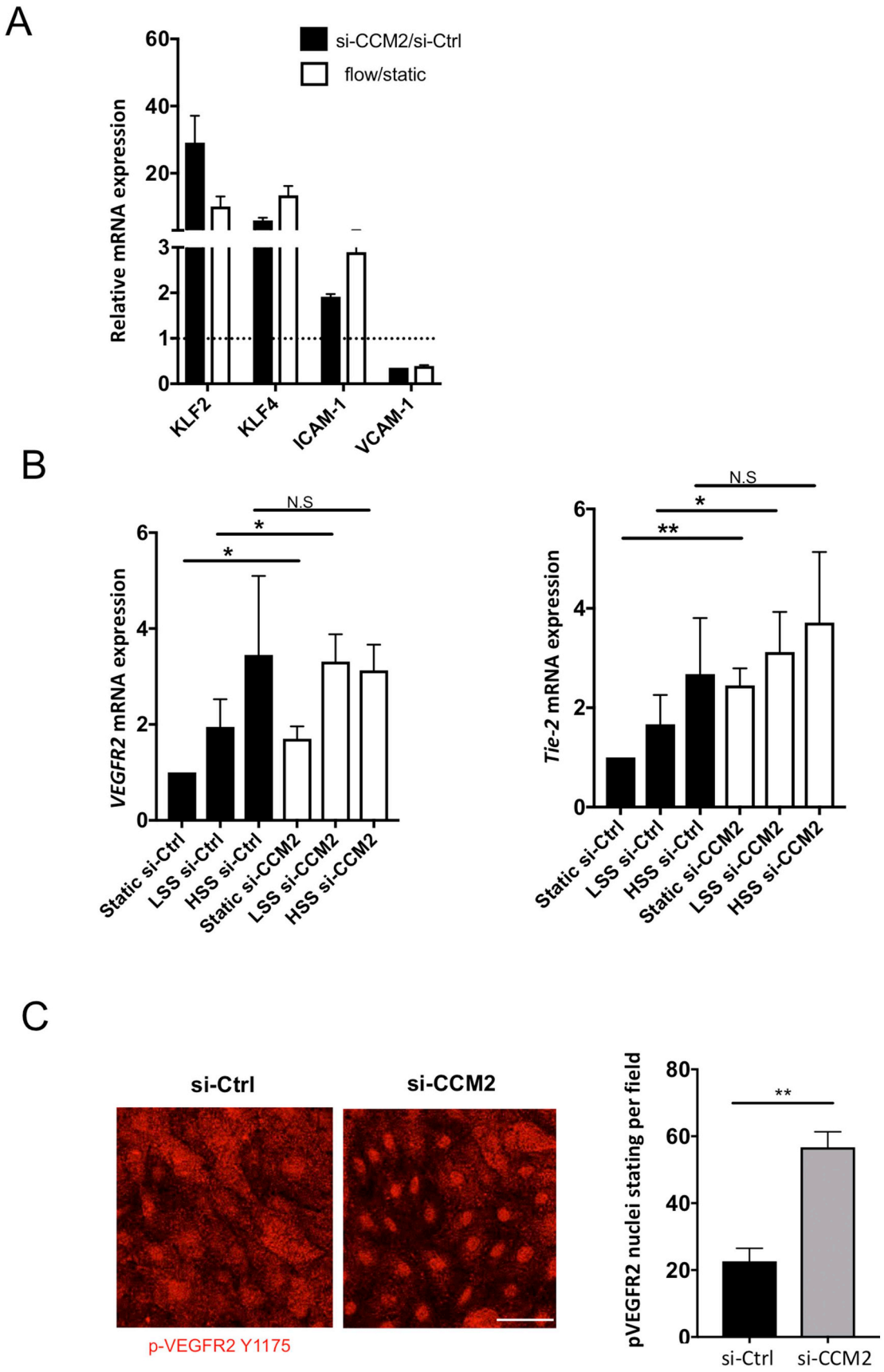

Fig. 8. Loss of CCM2 gene modulates molecular mechanosensor and enhances mechanotransduction sensitivity under LSS. (A) mRNA expression of *KLF2/4*, *ICAM-1* and *VCAM-1* under CCM2-silenced or FSS. (B) qPCR measurement of *TIE-2* and *VEGFR2* in control and CCM2-silenced EC under low and high FSS. (C) p-VEGFR2 staining in control or CCM2-silenced EC. Scale bars, 60 μm. Representative images are presented. n = 3 independent experiments. Data represent mean ± SD. *P < 0.05, **P < 0.01, determined by Student's *t*-test.

Lastly, other pathways, including the insulin, WNT, mTOR and c-MET pathways were also highly regulated in CCM2-silenced ECs under LSS but not under HSS suggesting their involvement in CCM mediated signalling. Indeed, mTOR and defective autophagy have been previously shown to be involved in CCM development [76]. Further studies to confirm the other potential signalling pathways and the scope of the immune response in CCM pathologies are required.

Collectively, our data demonstrates that loss of CCM may reset the response of ECs to LSS in part through altering the mechanosensory complex. Indeed, the CCM complex has been shown to be directly linked to key mechanosensory complex molecules such as VE-cadherin and VEGFR2 [4,77]. We would argue that CCM2 is essential for this complex to fine-tune its activity and respond appropriately to the LSS that is seen in the capillary-venous vessels in retina and brain [28,65,66]. Thus, our results suggest that the LSS that is seen in the CNS, in the absence of a functional CCM complex, contributes to the site-restricted development of CCM lesions.

Transparency document

The Transparency document associated with this article can be found, in online version.

Acknowledgments

We thank Julie Hunter for isolation of HUVECs and Prof Georges Grau, School of Medical Science, Bosch Institute, University of Sydney for providing hCMEC/D3 cells.

Sources of funding

This research was supported by grants from the National Health and Medical Research Council (NHMRC) of Australia #571408 (JRG), #1074664 (JL). JL holds NHMRC/Gustav Nossal Award. JRG holds the Wenkart Chair of the Endothelium at the Centenary Institute and the Sydney Medical School, University of Sydney.

Author contributions

JRG and JL conceived, designed, and led the project. JL performed most of the experiments and data analysis. YZ, PC, JC, KT and JC performed parts of the experiments and data analysis with assistance from XZ. JL, MAV and JRG wrote the manuscript with input from all authors.

Declaration of competing interest

The authors have declared that no conflict of interest exists.

Appendix A. Supplementary data

Supplementary data to this article can be found online at https://doi.org/10.1016/j.bbadis.2019.07.013.

References

[1] G. Boulday, N. Rudini, L. Maddaluno, A. Blecon, M. Arnould, A. Gaudric, et al., Developmental timing of ccm2 loss influences cerebral cavernous malformations in mice, J. Exp. Med. 208 (2011) 1835–1847.
[2] R.A. Stockton, R. Shenkar, I.A. Awad, M.H. Ginsberg, Cerebral cavernous malformations proteins inhibit rho kinase to stabilize vascular integrity, J. Exp. Med. 207 (2010) 881–896.
[3] J. Lisowska, C.J. Rodel, S. Manet, Y.A. Miroshnikova, C. Boyault, E. Planus, et al., The ccm1-ccm2 complex controls complementary functions of rock1 and rock2 that are required for endothelial integrity, J. Cell Sci. 131 (2018).
[4] A. Glading, J. Han, R.A. Stockton, M.H. Ginsberg, Krit-1/ccm1 is a rap1 effector that regulates endothelial cell-cell junctions, J. Cell Biol. 179 (2007) 247–254.
[5] L. Maddaluno, N. Rudini, R. Cuttano, L. Bravi, C. Giampietro, M. Corada, et al., Endmt contributes to the onset and progression of cerebral cavernous malformations, Nature. 498 (2013) 492–496.
[6] S. Yadla, P.M. Jabbour, R. Shenkar, C. Shi, P.G. Campbell, I.A. Awad, Cerebral cavernous malformations as a disease of vascular permeability: from bench to bedside with caution, Neurosurg. Focus. 29 (2010) E4.
[7] T.M. Mleynek, A.C. Chan, M. Redd, C.C. Gibson, C.T. Davis, D.S. Shi, et al., Lack of ccm1 induces hypersprouting and impairs response to flow, Hum. Mol. Genet. 23 (2014) 6223–6234.
[8] C. Hahn, M.A. Schwartz, Mechanotransduction in vascular physiology and atherogenesis, Nat. Rev. Mol. Cell Biol. 10 (2009) 53–62.
[9] Y.X. Qi, J. Jiang, X.H. Jiang, X.D. Wang, S.Y. Ji, Y. Han, et al., Pdgf-bb and tgf-{beta}1 on cross-talk between endothelial and smooth muscle cells in vascular remodeling induced by low shear stress, Proc. Natl. Acad. Sci. U. S. A. 108 (2011) 1908–1913.
[10] R.J. Dekker, R.A. Boon, M.G. Rondaij, A. Kragt, O.L. Volger, Y.W. Elderkamp, et al., Klf2 provokes a gene expression pattern that establishes functional quiescent differentiation of the endothelium, Blood. 107 (2006) 4354–4363.
[11] A. Hamik, Z. Lin, A. Kumar, M. Balcells, S. Sinha, J. Katz, et al., Kruppel-like factor 4 regulates endothelial inflammation, J. Biol. Chem. 282 (2007) 13769–13779.
[12] N. Baeyens, C. Bandyopadhyay, B.G. Coon, S. Yun, M.A. Schwartz, Endothelial fluid shear stress sensing in vascular health and disease, J. Clin. Invest. 126 (2016) 821–828.
[13] S.F. Retta, A.J. Glading, Oxidative stress and inflammation in cerebral cavernous malformation disease pathogenesis: two sides of the same coin, Int. J. Biochem. Cell Biol. 81 (2016) 254–270.
[14] Z. Zhou, A.T. Tang, W.Y. Wong, S. Bamezai, L.M. Goddard, R. Shenkar, et al., Cerebral cavernous malformations arise from endothelial gain of mekk3-klf2/4 signalling, Nature. 532 (2016) 122–126.
[15] J.A. Young, K.K. Ting, J. Li, T. Moller, L. Dunn, Y. Lu, et al., Regulation of vascular leak and recovery from ischemic injury by general and ve-cadherin-restricted mirna antagonists of mir-27, Blood. 122 (2013) 2911–2919.
[16] R. Jambou, V. Combes, M.J. Jambou, B.B. Weksler, P.O. Couraud, G.E. Grau, Plasmodium falciparum adhesion on human brain microvascular endothelial cells involves transmigration-like cup formation and induces opening of intercellular junctions, PLoS Pathog. 6 (2010) e1001021.
[17] P.R. Coleman, G. Chang, G. Hutas, M. Grimshaw, M.A. Vadas, J.R. Gamble, Age-associated stresses induce an anti-inflammatory senescent phenotype in endothelial cells, Aging (Albany NY) 5 (2013) 913–924.
[18] L. Yang, R.M. Froio, T.E. Sciuto, A.M. Dvorak, R. Alon, F.W. Luscinskas, Icam-1 regulates neutrophil adhesion and transcellular migration of tnf-alpha-activated vascular endothelium under flow, Blood. 106 (2005) 584–592.
[19] H. Oh, B. Siano, S. Diamond, Neutrophil isolation protocol, J. Vis. Exp. 17 (2008) 745.
[20] W.J. Polacheck, M.L. Kutys, J. Yang, J. Eyckmans, Y. Wu, H. Vasavada, et al., A non-canonical notch complex regulates adherens junctions and vascular barrier function, Nature. 552 (2017) 258–262.
[21] J. Huynh, N. Nishimura, K. Rana, J.M. Peloquin, J.P. Califano, C.R. Montague, et al., Age-related intimal stiffening enhances endothelial permeability and leukocyte transmigration, Sci. Transl. Med. 3 (2011) 112ra122.
[22] A.F. Guinan, K.D. Rochfort, P.A. Fitzpatrick, T.G. Walsh, A.R. Pierotti, S. Phelan, et al., Shear stress is a positive regulator of thimet oligopeptidase (ec3.4.24.15) in vascular endothelial cells: consequences for mhc1 levels, Cardiovasc. Res. 99 (2013) 545–554.
[23] J. Hwang, M.H. Ing, A. Salazar, B. Lassegue, K. Griendling, M. Navab, et al., Pulsatile versus oscillatory shear stress regulates nadph oxidase subunit expression: implication for native ldl oxidation, Circ. Res. 93 (2003) 1225–1232.
[24] J. Li, D.M. Sze, R.D. Brown, M.J. Cowley, W. Kaplan, S.L. Mo, et al., Clonal expansions of cytotoxic t cells exist in the blood of patients with waldenstrom macroglobulinemia but exhibit anergic properties and are eliminated by nucleoside analogue therapy, Blood. 115 (2010) 3580–3588.
[25] J. Wustehube, A. Bartol, S.S. Liebler, R. Brutsch, Y. Zhu, U. Felbor, et al., Cerebral cavernous malformation protein ccm1 inhibits sprouting angiogenesis by activating delta-notch signaling, Proc. Natl. Acad. Sci. U. S. A. 107 (2010) 12640–12645.
[26] M.O. Bernabeu, M.L. Jones, J.H. Nielsen, T. Kruger, R.W. Nash, D. Groen, et al., Computer simulations reveal complex distribution of haemodynamic forces in a mouse retina model of angiogenesis, J. R. Soc. Interface 11 (2014).
[27] N. Baeyens, B. Larrivee, R. Ola, B. Hayward-Piatkowskyi, A. Dubrac, B. Huang, et al., Defective fluid shear stress mechanotransduction mediates hereditary hemorrhagic telangiectasia, J. Cell Biol. 214 (2016) 807–816.
[28] S. Chatterjee, Endothelial mechanotransduction, redox signaling and the regulation of vascular inflammatory pathways, Front. Physiol. 9 (2018).
[29] M. Renz, C. Otten, E. Faurobert, F. Rudolph, Y. Zhu, G. Boulday, et al., Regulation of beta1 integrin-klf2-mediated angiogenesis by ccm proteins, Dev. Cell 32 (2015) 181–190.
[30] C. Otten, J. Knox, G. Boulday, M. Eymery, M. Haniszewski, M. Neuenschwander, et al., Systematic pharmacological screens uncover novel pathways involved in cerebral cavernous malformations, Embo. Mol. Med. 10 (2018).
[31] Y. He, H. Zhang, L. Yu, M. Gunel, T.J. Boggon, H. Chen, et al., Stabilization of vegfr2 signaling by cerebral cavernous malformation 3 is critical for vascular development, Sci. Signal. 3 (2010) ra26.
[32] D.E. Conway, M.T. Breckenridge, E. Hinde, E. Gratton, C.S. Chen, M.A. Schwartz, Fluid shear stress on endothelial cells modulates mechanical tension across ve-cadherin and pecam-1, Curr. Biol. 23 (2013) 1024–1030.
[33] M.A. Lopez-Ramirez, G. Fonseca, H.A. Zeineddine, R. Girard, T. Moore, A. Pham, et al., Thrombospondin1 (tsp1) replacement prevents cerebral cavernous malformations, J. Exp. Med. 214 (11) (2017) 3331–3346.

[34] Z. Zhou, D.R. Rawnsley, L.M. Goddard, W. Pan, X.J. Cao, Z. Jakus, et al., The cerebral cavernous malformation pathway controls cardiac development via regulation of endocardial mekk3 signaling and klf expression, Dev. Cell 32 (2015) 168–180.

[35] J. Liu, X. Bi, T. Chen, Q. Zhang, S.X. Wang, J.J. Chiu, et al., Shear stress regulates endothelial cell autophagy via redox regulation and sirt1 expression, Cell Death Dis. 6 (2015) e1827.

[36] Z. Mai, Z. Peng, S. Wu, J. Zhang, L. Chen, H. Liang, et al., Single bout short duration fluid shear stress induces osteogenic differentiation of mc3t3-e1 cells via integrin beta1 and bmp2 signaling cross-talk, PLoS One 8 (2013) e61600.

[37] R.K. Wolfson, B. Mapes, J.G.N. Garcia, Excessive mechanical stress increases hmgb1 expression in human lung microvascular endothelial cells via stat3, Microvasc. Res. 92 (2014) 50–55.

[38] D. van Breevoort, E.L. van Agtmaal, B.S. Dragt, J.K. Gebbinck, I. Dienava-Verdoold, A. Kragt, et al., Proteomic screen identifies igfbp7 as a novel component of endothelial cell-specific weibel-palade bodies, J. Proteome Res. 11 (2012) 2925–2936.

[39] A.T. Tang, J.P. Choi, J.J. Kotzin, Y. Yang, C.C. Hong, N. Hobson, et al., Endothelial tlr4 and the microbiome drive cerebral cavernous malformations, Nature. 545 (2017) 305–310.

[40] L. Bravi, N. Rudini, R. Cuttano, C. Giampietro, L. Maddaluno, L. Ferrarini, et al., Sulindac metabolites decrease cerebrovascular malformations in ccm3-knockout mice, Proc. Natl. Acad. Sci. U. S. A. 112 (2015) 8421–8426.

[41] B. Opitz, J. Eitel, K. Meixenberger, N. Suttorp, Role of toll-like receptors, nod-like receptors and rig-i-like receptors in endothelial cells and systemic infections, Thromb. Haemost. 102 (2009) 1103–1109.

[42] R. Caruso, N. Warner, N. Inohara, G. Nunez, Nod1 and nod2: signaling, host defense, and inflammatory disease, Immunity. 41 (2014) 898–908.

[43] J.L. Pomerantz, D. Baltimore, Nf-kappab activation by a signaling complex containing traf2, tank and tbk1, a novel ikk-related kinase, EMBO J. 18 (1999) 6694–6704.

[44] M. Katoh, M. Katoh, Integrative genomic analyses on hes/hey family: notch-independent hes1, hes3 transcription in undifferentiated es cells, and notch-dependent hes1, hes5, hey1, hey2, heyl transcription in fetal tissues, adult tissues, or cancer, Int. J. Oncol. 31 (2007) 461–466.

[45] S. Takeshita, N. Inoue, T. Ueyama, S. Kawashima, M. Yokoyama, Shear stress enhances glutathione peroxidase expression in endothelial cells, Biochem. Biophys. Res. Commun. 273 (2000) 66–71.

[46] A.H. Wagner, O. Kautz, K. Fricke, M. Zerr-Fouineau, E. Demicheva, B. Guldenzoph, et al., Upregulation of glutathione peroxidase offsets stretch-induced proatherogenic gene expression in human endothelial cells, Arterioscler. Thromb. Vasc. Biol. 29 (2009) 1894–1901.

[47] P. Arjunan, X. Lin, Z. Tang, Y. Du, A. Kumar, L. Liu, et al., Vegf-b is a potent antioxidant, Proc. Natl. Acad. Sci. U. S. A. 115 (2018) 10351–10356.

[48] R.D. Fontijn, O.L. Volger, J.O. Fledderus, A. Reijerkerk, H.E. de Vries, A.J.G. Horrevoets, Sox-18 controls endothelial-specific claudin-5 gene expression and barrier function, Am J Physiol-Heart C. 294 (2008) H891–H900.

[49] A. Abramsson, P. Lindblom, C. Betsholtz, Endothelial and nonendothelial sources of pdgf-b regulate pericyte recruitment and influence vascular pattern formation in tumors, J. Clin. Invest. 112 (2003) 1142–1151.

[50] J. Seebach, P. Dieterich, F. Luo, H. Schillers, D. Vestweber, H. Oberleithner, et al., Endothelial barrier function under laminar fluid shear stress, Lab. Investig. 80 (2000) 1819–1831.

[51] Ibidi gmbh, shear stress and shear rates for μ-slides y-shaped based on computational fluid dynamics (cfd). Application note 18: Https://ibidi.Com/img/cms/support/an/an18_shear_stress_y_shaped.Pdf. Access date: 23rd july 2018.

[52] L. Goitre, F. Balzac, S. Degani, P. Degan, S. Marchi, P. Pinton, et al., Krit1 regulates the homeostasis of intracellular reactive oxygen species, PLoS One 5 (2010) e11786.

[53] L. Goitre, P.V. DiStefano, A. Moglia, N. Nobiletti, E. Baldini, L. Trabalzini, et al., Up-regulation of nadph oxidase-mediated redox signaling contributes to the loss of barrier function in krit1 deficient endothelium, Sci. Rep. 7 (2017) 8296.

[54] K.S. Heo, K. Fujiwara, J. Abe, Disturbed-flow-mediated vascular reactive oxygen species induce endothelial dysfunction, Circ. J. 75 (2011) 2722–2730.

[55] A.L. Mowbray, D.H. Kang, S.G. Rhee, S.W. Kang, H. Jo, Laminar shear stress up-regulates peroxiredoxins (prx) in endothelial cells: Prx 1 as a mechanosensitive antioxidant, J. Biol. Chem. 283 (2008) 1622–1627.

[56] T. Nagel, N. Resnick, W.J. Atkinson, C.F. Dewey Jr., M.A. Gimbrone Jr., Shear stress selectively upregulates intercellular adhesion molecule-1 expression in cultured human vascular endothelial cells, J. Clin. Invest. 94 (1994) 885–891.

[57] A. Ohtsuka, J. Ando, R. Korenaga, A. Kamiya, N. Toyama-Sorimachi, M. Miyasaka, The effect of flow on the expression of vascular adhesion molecule-1 by cultured mouse endothelial cells, Biochem. Biophys. Res. Commun. 193 (1993) 303–310.

[58] E. Tzima, M. Irani-Tehrani, W.B. Kiosses, E. Dejana, D.A. Schultz, B. Engelhardt, et al., A mechanosensory complex that mediates the endothelial cell response to fluid shear stress, Nature 437 (2005) 426–431.

[59] L.F. de Castro, M. Maycas, B. Bravo, P. Esbrit, A. Gortazar, VEGF Receptor 2 (VEGFR2) Activation Is Essential for Osteocyte Survival Induced by Mechanotransduction, J. Cell. Physiol. 230 (2) (2015) 278–285.

[60] L.K. Tai, Q. Zheng, S. Pan, Z.G. Jin, B.C. Berk, Flow activates erk1/2 and endothelial nitric oxide synthase via a pathway involving pecam1, shp2, and tie2, J. Biol. Chem. 280 (2005) 29620–29624.

[61] Z. Macek Jilkova, J. Lisowska, S. Manet, C. Verdier, V. Deplano, C. Geindreau, et al., Ccm proteins control endothelial beta1 integrin dependent response to shear stress, Biol. Open. 3 (2014) 1228–1235.

[62] A. Shay-Salit, M. Shushy, E. Wolfovitz, H. Yahav, F. Breviario, E. Dejana, et al., Vegf receptor 2 and the adherens junction as a mechanical transducer in vascular endothelial cells, Proc. Natl. Acad. Sci. U. S. A. 99 (2002) 9462–9467.

[63] R. Cuttano, N. Rudini, L. Bravi, M. Corada, C. Giampietro, E. Papa, et al., Klf4 is a key determinant in the development and progression of cerebral cavernous malformations, Embo. Mol. Med. 8 (2016) 6–24.

[64] G.B. Schulz, E. Wieland, J. Wustehube-Lausch, G. Boulday, I. Moll, E. Tournier-Lasserve, et al., Cerebral cavernous malformation-1 protein controls dll4-notch3 signaling between the endothelium and pericytes, Stroke. 46 (2015) 1337–1343.

[65] E. Mairey, A. Genovesio, E. Donnadieu, C. Bernard, F. Jaubert, E. Pinard, et al., Cerebral microcirculation shear stress levels determine neisseria meningitidis attachment sites along the blood-brain barrier, J. Exp. Med. 203 (2006) 1939–1950.

[66] S.S. Shaik, T.D. Soltau, G. Chaturvedi, B. Totapally, J.S. Hagood, W.W. Andrews, et al., Low intensity shear stress increases endothelial elr+ cxc chemokine production via a focal adhesion kinase-p38{beta} mapk-nf-{kappa}b pathway, J. Biol. Chem. 284 (2009) 5945–5955.

[67] S. Donat, M. Lourenco, A. Paolini, C. Otten, M. Renz, S. Abdelilah-Seyfried, Heg1 and ccm1/2 proteins control endocardial mechanosensitivity during zebrafish valvulogenesis, Elife. 7 (2018).

[68] G. Tanriover, B. Sozen, A. Seker, T. Kilic, M. Gunel, N. Demir, Ultrastructural analysis of vascular features in cerebral cavernous malformations, Clin. Neurol. Neurosurg. 115 (2013) 438–444.

[69] O. Dumont, L. Loufrani, D. Henrion, Key role of the no-pathway and matrix metalloprotease-9 in high blood flow-induced remodeling of rat resistance arteries, Arterioscler. Thromb. Vasc. Biol. 27 (2007) 317–324.

[70] R.A. Boon, T. Seeger, S. Heydt, A. Fischer, E. Hergenreider, A.J. Horrevoets, et al., Microrna-29 in aortic dilation: implications for aneurysm formation, Circ. Res. 109 (2011) 1115–1119.

[71] R.D. Rudic, E.G. Shesely, N. Maeda, O. Smithies, S.S. Segal, W.C. Sessa, Direct evidence for the importance of endothelium-derived nitric oxide in vascular remodeling, J. Clin. Invest. 101 (1998) 731–736.

[72] J.S. Mondy, V. Lindner, J.K. Miyashiro, B.C. Berk, R.H. Dean, R.L. Geary, Platelet-derived growth factor ligand and receptor expression in response to altered blood flow in vivo, Circ. Res. 81 (1997) 320–327.

[73] K. Gaengel, G. Genove, A. Armulik, C. Betsholtz, Endothelial-mural cell signaling in vascular development and angiogenesis, Arterioscler. Thromb. Vasc. Biol. 29 (2009) 630–638.

[74] A. Quaegebeur, I. Segura, P. Carmeliet, Pericytes: blood-brain barrier safeguards against neurodegeneration? Neuron. 68 (2010) 321–323.

[75] E. Faurobert, C. Albiges-Rizo, Recent insights into cerebral cavernous malformations: a complex jigsaw puzzle under construction, FEBS J. 277 (2010) 1084–1096.

[76] S. Marchi, M. Corricelli, E. Trapani, L. Bravi, A. Pittaro, S. Delle Monache, et al., Defective autophagy is a key feature of cerebral cavernous malformations, Embo. Mol. Med. 7 (2015) 1403–1417.

[77] P.V. DiStefano, J.M. Kuebel, I.H. Sarelius, A.J. Glading, Krit1 protein depletion modifies endothelial cell behavior via increased vascular endothelial growth factor (vegf) signaling, J. Biol. Chem. 289 (2014) 33054–33065.